Applied Catalysis B: Environmental 223 (2018) 116–124

Contents lists available at ScienceDirect

Applied Catalysis B: Environmental

journal homepage: www.elsevier.com/locate/apcatb

Effect of support material Al_2O_3 *vs* ZrO_2-TiO_2 on the Ba availability for NSR catalyst: An *in situ* and *operando* IR study

Sandra Palma Del Valle[a], Olivier Marie[a,*], Hai P. Nguyen[b]

[a] Normandie Univ., ENSICAEN, UNICAEN, CNRS, Laboratoire Catalyse et Spectrochimie, 14000 Caen, France
[b] Catalyst Research/Advanced Technology, Toyota Motor Europe NV/SA, Hoge wei 33, B-1930 Zaventem, Belgium

ARTICLE INFO

Article history:
Received 30 September 2016
Received in revised form 25 January 2017
Accepted 14 February 2017
Available online 20 February 2017

Keywords:
NSR catalysis
Alumina
Zirconia
Titanium oxide
Ba coverage
Adsorption kinetics
Operando spectroscopy

ABSTRACT

The evolution of Ba sites in two distinct NOx storage and reduction (NSR) catalysts that are based on alumina or zirconia-titania mixed oxide (ZrO_2-TiO_2 or ZT) during NOx adsorption/desorption was investigated by *in situ* and *operando* IR spectroscopy. Based on various evidences from the *in situ* study, medium sized Ba sites on alumina supported fresh catalysts are proposed to experience sintering under NOx adsorption to form bigger particles, while for ZT, initially possessing smaller sized Ba particles, the formation of a thin layer or very fine particles of Ba would proceed under the same condition. This evolution can also be affirmed by observations from the *operando* IR study showing that NOx adsorption on ZT supported catalyst is initially faster than on alumina supported catalyst (time on stream lower than 300 s), but after long adsorption time (about 50 min) the two catalysts show similar storage capacity. This new mechanistic insight suggests that NOx ad/desorption rate, which is critical for optimizing NSR performance, needs to be controlled by support materials whose interaction with the Ba particles not only determines their initial size (fresh catalyst) but also their resistance towards sintering during the NOx adsorption

1. Introduction

Lean-burn engine technology is a promising solution to increase the fuel efficiency and decrease the emission of greenhouse gases as carbon dioxide and hydrocarbons [1]. However, the formed NOx cannot be effectively reduced to N_2 over traditional three-ways catalysts (TWCs) [2]. The NOx storage and reduction technique (NSR) was firstly proposed by Toyota Motor Company as a promising after-treatment process for Diesel engines [3] but could also be useful for lean-burn engines. NSR catalysts are usually made of three major components: a precious metal (*e.g.* Pt and/or Pd and/or Rh), an alkali or alkaline earth metal oxide as a storage material (*e.g.* Ba, Sr, Li, Ca, K or Na), and a support with high surface area such as γ-Al_2O_3 [4].

In the NOx storage and reduction reaction, NO (g) is initially oxidized to NO_2 (g) on the noble metal under lean conditions, followed by the formation of nitrites and nitrates on the storage materials. Finally, under rich conditions stored species are reduced to N_2 (g).

All these processes are performed in cycles, the storage duration is of the order of a few minutes, while the reduction duration is in the order of 1–20 s.

Pt-Ba/Al_2O_3 has been the most studied NSR catalyst formulation and a comprehensive review of the knowledge accumulated till 2004 has been presented by Epling et al. [5]. The first mechanism proposed for this catalyst assumes that NOx species are stored on BaO or $BaCO_3$ but further studies have shown that NOx storage can occur not only on the BaO component but also on the γ-Al_2O_3 support [6–8].

The NSR catalysts deactivate due to sulfur-poisoning and/or thermal deterioration [5]. The sulfur content poisons the precious metals [9], the supports [10] and the NOx storage materials [9]. It has been confirmed that the adsorbed sulfur transforms the NOx storage materials into sulfates [2,9–11]. The sulfates and the desorbed sulfur compound decompose into sulfur oxides or hydrogen sulfide when the temperature goes above 873 K under rich condition, thus partially restoring the NO_x storage ability [9,12,13]. An effective strategy to improve the sulfur tolerance was the use of titanium dioxide (TiO_2). Matsumoto et al. found that the decomposition temperature of sulfates on a TiO_2 support was lower than that on an Al_2O_3 support under reducing conditions [10]. The addition of ZrO_2 to TiO_2 produces an increment of the thermal stability of the catalytic material. Hachisuka et al. have also published that

* Corresponding author.
E-mail address: olivier.marie@ensicaen.fr (O. Marie).

http://dx.doi.org/10.1016/j.apcatb.2017.02.053
0926-3373/

a ZrO_2-TiO_2 (ZT) catalyst presents a better NSR activity that the separate oxides [14].

Preliminary results on Pt-Ba catalysts supported on different oxides also indicated different NO_x storage behavior depending on the support [15]. The present investigation thus aims at clarifying the interaction between the barium storing phase and the oxide support (either Al_2O_3 or ZT) in order to understand the distinct dynamic behaviors observed during the storing period. The novelty of our work thus lies in the detailed IR characterization of a new formulation Ba/ZT (mixed oxide) that has been little studied [16] and the comparison of its dynamic trapping behavior with a benchmark well known Ba/Al catalyst. To the best of our knowledge, such a study has never been reported.

For that purpose, IR spectroscopy represents a powerful technique being sensitive to the state of the adsorbed molecules and thus to the nature of the interacting site. Thanks to an '*in situ*' approach applied to study both the bare oxides or the Ba loaded formulations, it will be possible not only to identify the fingerprint *IR* bands typical for each adsorbed NOx species but also to quantify the total amount of adsorbed species for any given sample.

Furthermore, the catalytic formulations (Pt + Ba loaded oxides) will also be studied under duty (representative reaction temperature and flow conditions) applying the IR *operando* methodology in the transmittance mode which has recently been successful for the simulation of a Lean-NOx-Trap system [17]. The collected *operando* data will allow to obtain a correlation between the dynamics of the NOx trapping and the nature of the adsorbed species, provided the fluidodynamics resulting from the cell design is the most appropriate to carry out kinetic studies. In particular, in a recent work, Dujardin et al. pointed out that typical reactor-cell design presents drawbacks regarding the sample holder geometry [18]. As a consequence, a square shaped sample holder with inlet and outlet 'cone sprays' was recently designed [18] enabling to consider the pellet zone as a perfect Plug Flow Reactor (PFR) made of ten Continuously Stirred Tank Reactors (CSTR) in series. This configuration was used in the present study, being the most suited for quantitative analysis.

2. Experimental

2.1. *Catalysts*, in situ *and* operando *setup*

2.1.1. *Catalysts*

The $Pt/Ba/Al_2O_3$ and $Pt/Ba/ZrO_2$-TiO_2 lean NOx trap catalysts and the intermediate solids used in this study were supplied by Toyota. The composition of these solids are 1%wt Pt and 11% wt Ba onto ZrO_2-TiO_2 (70% ZrO_2–30% TiO_2) or γ-Al_2O_3 supports whose specific area are S_{BET} = 100 $m^2\ g^{-1}$ and S_{BET} = 200 $m^2\ g^{-1}$ respectively.

2.1.2. In situ *setup*

Material surface properties have been studied by *in situ* FT-IR spectroscopy of adsorbed probe molecules. The Fourier transform infrared (FTIR) spectra were recorded at room temperature on a Nicolet Nexus FTIR 5700 spectrometer (Thermo Scientific) equipped with a DTGS KBr detector and an extended KBr beam splitter at a spectral resolution of 4 cm^{-1} accumulating 128 scans. The powdered samples were pressed into thin self-supporting pellets of around 10 mg/cm^2 and placed in a vacuum quartz cell equipped with KBr windows, where they underwent all activation and adsorption treatments. The spectra were recorded at room temperature (RT).

Before the measurements, the samples were activated at 723 K (for 1.5 h) under high vacuum ($p = \sim 10^{-6}$ mbar). When carbonate traces remained on the surface after such a pre-treatment (barium containing samples), three cycles of storage, reduction and evacuation were performed (Eqs. (1)–(2)). One cycle consists in the introduction at 723 K of an NO_2 equilibrium pressure (1.33 mbar) in contact with the sample during 10 min, the setup is then evacuated and 133 mbar of H_2 are further introduced for another 10 min before evacuation. The FTIR spectra of the activated samples were subtracted from those recorded after NO_2 adsorption. All the spectra reported in the present work are the results of this subtraction and are normalized to a similar weight of sample.

$$BaCO_3 + 2NO_2 \rightarrow Ba(NO_3)_2 + CO_2 \quad (1)$$

$$Ba(NO_3)_2 + 5H_2 \rightarrow BaO + N_2 + 5\,H_2O \quad (2)$$

2.1.3. Operando *setup*

Whatever the oxide support, the catalyst powder was pressed in wafers with a thickness of about 50 μm. The square wafer, a 10.5 × 10.5 mm pellet, was inserted in a specifically designed sample holder with a triangular gas distributor (cone spray) and a triangular collector that was finally introduced in the *Sandwich* cell described in [17].

As indicated on Fig. 1, the cell was then connected to the gas manipulation apparatus, consisting of mass flow controllers in addition to a mass spectrometer (Pfeiffer Omnistar GSD 301), an IR gas cell (Thermo Scientific Nicolet iS50 GC-IR) and a complementary NO-NO_2-NOx chemiluminiscense analyser (Megatec 42i-HL Thermo Scientific) for the analysis of the gaseous phase leaving the reactor.

Infrared spectra (32 scans per spectrum) of both the catalyst and the gas phase were collected with an acquisition frequency of one spectrum every 2.7 s by means of a Thermo Scientific Nicolet iS50 FT-IR equipped with an MCT detector.

2.2. *Reaction conditions for* operando *FTIR study of NOx storage*

The NOx uptake experiments were carried out under lean fuel conditions at two different fixed temperatures. The samples were preliminary activated at 723 K under lean flow (0.2% NO mol 3.3% O_2 in Ar) for 90 min and then reduced during 3 min under 'rich flow conditions' (3.3% H_2/Ar). Meanwhile, the reaction flow (50 mLN min^{-1}) made of 400 ppm of NO_2 and 1% O_2 in Ar was stabilized and analysed. After activation, the reaction flow was sent to the sample.

The NOx trapped during the lean period after a τ duration under flow was calculated using the Eq. (3), taking into account the NOx fed and NOx out of the cell during the lean period:

$$[\text{NOx storage}](\tau) = \frac{\int_0^{\tau}[(F_{NOx}(in) - F_{NOx}(out)]dt}{w} \quad (3)$$

where F_{NOx} stands for the NOx molar flow rate and w for the catalyst weight.

The gas hourly space velocity (GHSV) used for the experiments based on the volume of the pressed materials was ca. 400,000 h^{-1}, so that the experiments were always performed using a similar ratio between flow and catalyst weight. Similar catalyst weights were even used for all the performed *operando* experiments.

3. Results and discussion

3.1. In situ NO_2 *adsorption*

3.1.1. Al_2O_3 *and* Ba/Al_2O_3

As advised in the introduction part, a preliminary requirement before performing IR *operando* experiments consists in the proper identification of the nature of the possible expected adsorbed species. For this purpose, the *in situ* approach allows to start the adsorption study from a catalyst surface free of remaining impurities thanks to a conjugated thermal and under vacuum pretreatment. Furthermore, the introduction of the probe molecule

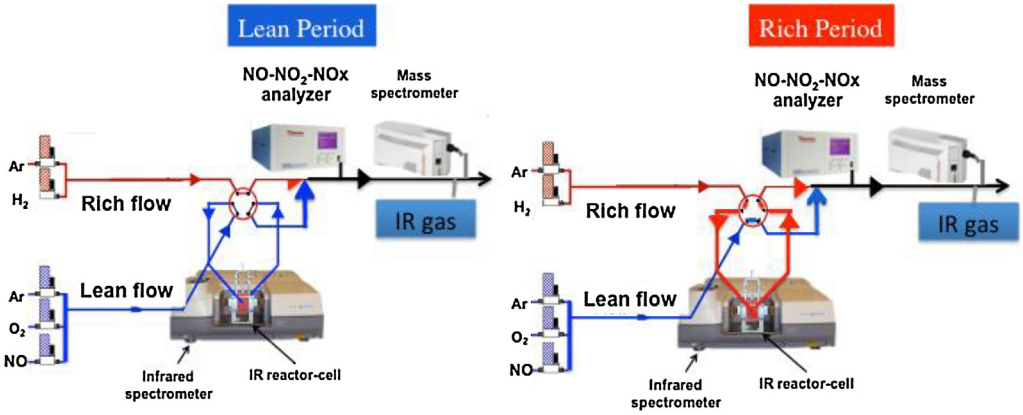

Fig. 1. Scheme of the operando setup either in the Lean flow (left part) or Rich pretreatment flow (right part) configuration.

(here NO_2) can be performed either through small dosed amounts or via a large excess (equilibrium pressure) and the stability of the formed adsorbed species may be tested upon a subsequent temperature programmed desorption (TPD) study. Indeed, the evolution of the IR spectra upon increasing adsorbed amounts (and thus contact time) may reveal preferential interaction sites while the thermal stability of the adsorbed species will also help to identify their coordination mode.

The study of NO_2 adsorption over alumina has already been widely reported [19–21] and the spectra are here reported mostly for comparison purpose with the Ba loaded sample. The Fig. 2 thus represents on the left part the evolution of the spectra obtained after adsorption of increasing amount of NO_2 over Al_2O_3 at room temperature. From the very first NO_2 dose, a lone band appears at about 1465 cm^{-1} that is assigned to the ν_{as} stretching mode for linear (monodentate) nitrite (NO_2^-). Its intensity reaches a plateau value after few supplementary doses and remains quite low upon increasing NO_2 amounts as nitrates species (NO_3^-) emerge. The two peaks related to the degenerated ν_{as} stretching mode for adsorbed NO_3^- which are first detected lie at 1564 and 1296 cm^{-1}. They are assigned to monodentate nitrates whose formation arises from an oxygen transfer to the linear NO_2^-. Then, two distinct pairs of bands appears whose intensities become majority above 0.99 mmol g^{-1}. The ν_{as} degenerated mode splits at 1580–1270 cm^{-1} for one species and at 1595–1245 cm^{-1} for the other one. These pairs of bands would thus both characterize bidentate NO_3^- whose formation proceeds onto distinct defect sites of the alumina surface. Finally, two shoulders are also clearly detected above 1600 cm^{-1}, *i.e* in the range where bridged NO_3^- species are expected. The lower wavenumber peaks associated with the split of the ν_{as} stretching mode for these bridged species is less obvious but a careful analysis of the spectra allows to couple the peaks as follows 1620–1230 cm^{-1} and 1660–1180 cm^{-1} for the two distinct bridged nitrates observed over our alumina support. These bands matches and assignments were checked upon TPD (see Supporting Information file) which confirmed the nature of the species according to their thermal stability in order: monodentate < bridged < bidentate.

As shown on Fig. 2 (right part), the impact of Ba loading leads to the appearance of new specific species while some IR bands typical for aluminum adsorption sites remain after a classical NO_2 adsorption at room temperature. The most striking feature of NO_2 adsorption over Ba/Al_2O_3 consists in a pair of broad and intense bands at about 1430–1330 cm^{-1} that appears from the very first doses. The high wavenumber component of this split ν_{as} degenerated mode (~1430 cm^{-1}) is completely absent for the bare alumina oxide and should thus characterize the barium phase. A careful analysis of the spectra even indicates that each broad component is indeed made of two peaks, so that finally two distinct species with the following IR signature 1441–1325 cm^{-1} and 1425–1331 cm^{-1} are formed. The rather low extent of the ν_a split ($\Delta\nu_{as} \approx 100$ cm^{-1}) suggests that the corresponding species are either Ba monodentate nitrates or Ba polydentate nitrates [22] while the exact assignment of one pair of band to a given species is hazardous even from the TPD data (see SI file). Two other bands are also easily detected in the low NOx coverage range, their intensity remaining low upon increasing NO_2 amounts. The first one at 1220 cm^{-1} is absent for the bare alumina support and characterizes Ba bridged NO_2^- while the second one lying at 1480 cm^{-1} would be typical for linear (monodentate) nitrite over Al perturbed by Ba in the neighborhood. An issue now arises regarding the nature of the interacting sites for a correct assignment of the rest of the peaks detected over the Ba/Al_2O_3 sample since they are all close to peaks already observed for the bare Al_2O_3 support. For example, one species characterized by a pair of bands at 1590–1295 cm^{-1} is detected for the Ba loaded sample while similar peaks were previously detected at 1580–1270 cm^{-1} for the bare alumina oxide. The peaks position clearly reveals that in both cases bidentate nitrates are formed but for the Ba/Al_2O_3 sample does the interaction takes place with an Al or a Ba cationic site? Based on the fact that for BaO loading above 8 wt% onto an alumina support presenting a 160 m^2 g^{-1} specific area, a barium monolayer is expected [23], some authors assign the whole bands observed over Ba/Al_2O_3 to NO_x involving interaction with Ba sites [8,23]. However, since the formation of a Ba monolayer over the alumina support may depend on many parameters such as the temperature of the preliminary calcination of the alumina, its surface hydration, its specific area (here 200 m^2 g^{-1}), it was decided in the present work to find a mean to distinguish the support from the Ba adsorption sites. For that purpose, the NO_2 adsorption experiment over Ba/Al_2O_3 was repeated but the sample was now heated at 653 K for 5 min between each introduction of dosed NO_2 aliquot. The heating temperature of 653 K was chosen high enough to provide the energy for diffusion and interaction with bulk Ba sites but also low enough to keep the thermodynamics in favor of NO_2 (with regards to its decomposition to NO +O_2). This methodology was inspired from an elegant work by Szanyi et al. [24,25] who showed a change in the proportion of bulk Ba site upon heating under a NO_2 atmosphere. The Fig. 3 represents a comparison between the two spectra obtained after NO_2 saturation of the Ba/Al_2O_3 sample with or without heating at 653 K. It is thus obvious that the heating treatment provokes an increase of the proportion of pure Ba nitrates as revealed by the increase of the monodentate and/or polydentate peaks at about 1430–1330 cm^{-1} at the expense of the bidentate peaks (1590–1295 cm^{-1}) but also bridged species bands (1640–1250 cm^{-1} and 1612–1264 cm^{-1}, not discussed yet).

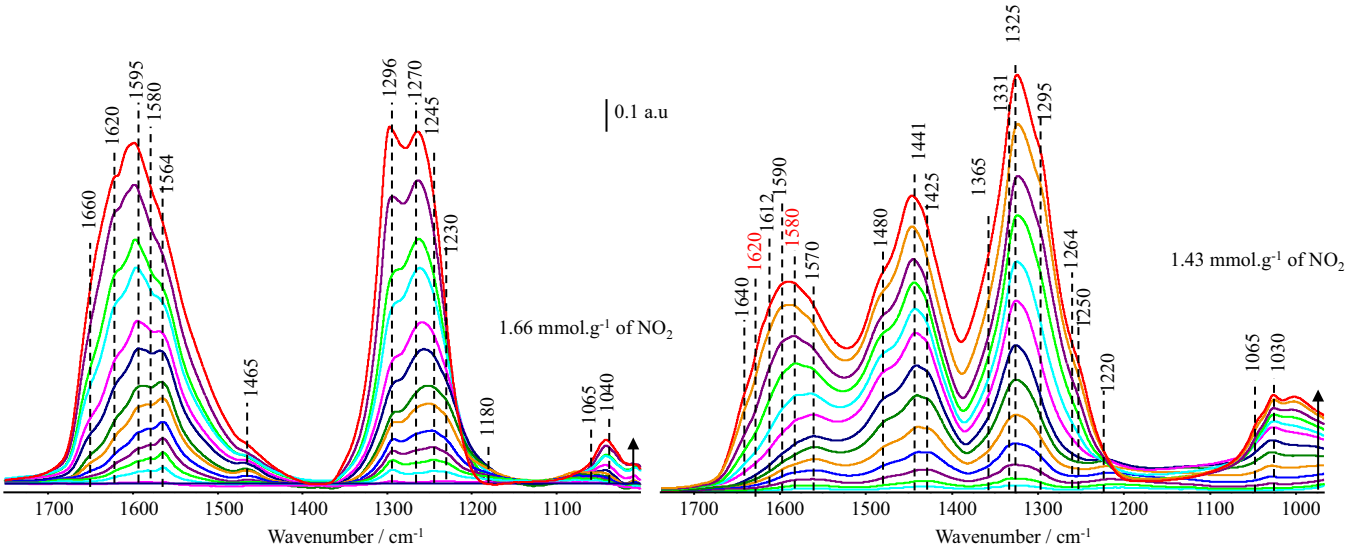

Fig. 2. Evolution of the spectra upon increasing NO_2 amount at 293 K over Al_2O_3 support (Left part) or Ba/Al_2O_3 (Right part). Incremental doses of about 0.11 mmol g^{-1} were introduced till a value of about 1.5 mmol g^{-1}. (Note: NO_2 amounts indicated on the graph correspond to the value relative to the last spectrum shown, not to the saturation level of the catalysts).

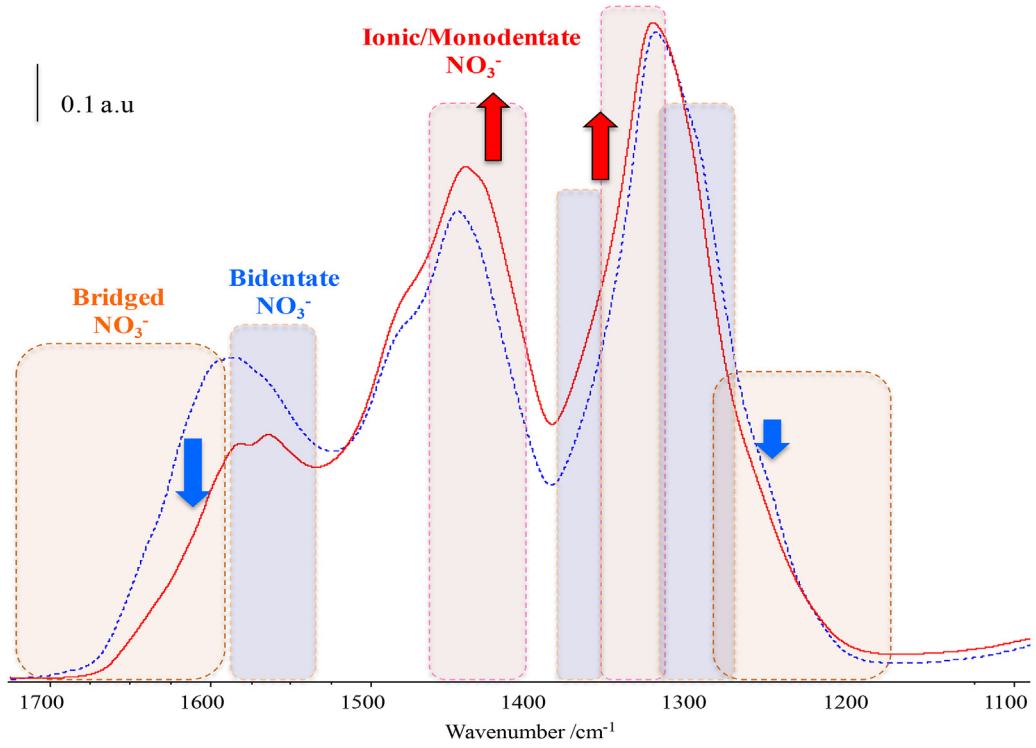

Fig. 3. Comparison of the spectra obtained after introduction of 1.4 mmol g^{-1} of NO_2 over Ba/Al_2O_3 either at 293 K (– – – –) or after heating at 653 K (·····).

Since, the heating in presence of NO_2 was reported to lead to a redistribution of medium sized Ba particles into bigger Ba clusters that form simultaneously with a thin Ba monolayer over the alumina support [25], it is not only expected that the proportion of exposed Ba sites rises but also that the amount of superficial alumina sites decreases. As a consequence, we propose that the pair of bands present at 1590–1295 cm^{-1} but also that at 1570–1365 cm^{-1} characterize distinct bidentate species interacting with different Al cationic site from the oxide support (most probably perturbed by the presence of surrounding Ba). In a similar way, the pairs of bands at 1640–1250 cm^{-1} and 1612–1264 cm^{-1} necessarily characterize bridged NO_3^- species involving either only aluminum cations or most probably both Al and Ba cations (interfacial sites). For clarity sake, Table 1 provides a summary of the peaks detected in the present work and their proposed assignments.

3.1.2. *ZrO_2-TiO_2 and Ba/ZrO_2-TiO_2*

In a similar way, the NO_2 adsorption was performed on ZrO_2-TiO_2 and Ba/ZrO_2-TiO_2 for comparison purpose (Fig. 4).

Concerning the bare ZrO_2-TiO_2 support (Fig. 4 left part), one main broad band is detected at about 1185 cm^{-1} in the low coverage level range. The intensity of this band goes through a maximum upon increasing NO_2 amount and finally vanishes at high coverage level. This behavior is typical for nitrites species that are known to

Table 1
A summary of band assignments for IR vibrations detected upon NO_2 adsorption over Ba free or Ba loaded Al_2O_3 and ZrO_2-TiO_2 oxide supports.

Catalyst	Infrared bands and their assignments/cm^{-1}							
	Bridged nitrate		Bidentate nitrate		Monodentate/ionic nitrate		Linear nitrite	Bridged nitrite
Al_2O_3	1660 1620	1180 1230	1595 1580	1245 1270	1564	1296	1465	
Ba/Al_2O_3	1640[a] 1612[a]	1250[a] 1264[a]	1590[b] 1570[b]	1295[b] 1365[b]	1441* 1425*	1325* 1331*	1475–1480[b]	1220–1230[b]
ZrO_2-TiO_2	1650 1620	1200 1215	1615 1582	1230 1244	1550[c] 1515 1485	1285[c] 1300 1310		1183
Ba/ZrO_2-TiO_2	1620[d] 1612[d]	1225[d] 1180[d]	1579[d] 1520	1297[d] 1239	1480* 1436* 1417* 1400*	1300* 1369* 1357* 1337*	1450[d]	1209[d]

* Species on BaO.
[a] Species on interface Al-Ba.
[b] Species on Al perturbed by surrounding Ba.
[c] Species on TiO_2 phase.
[d] Species on ZrO_2-TiO_2 perturbed by surrounding Ba or involving Ba sites.

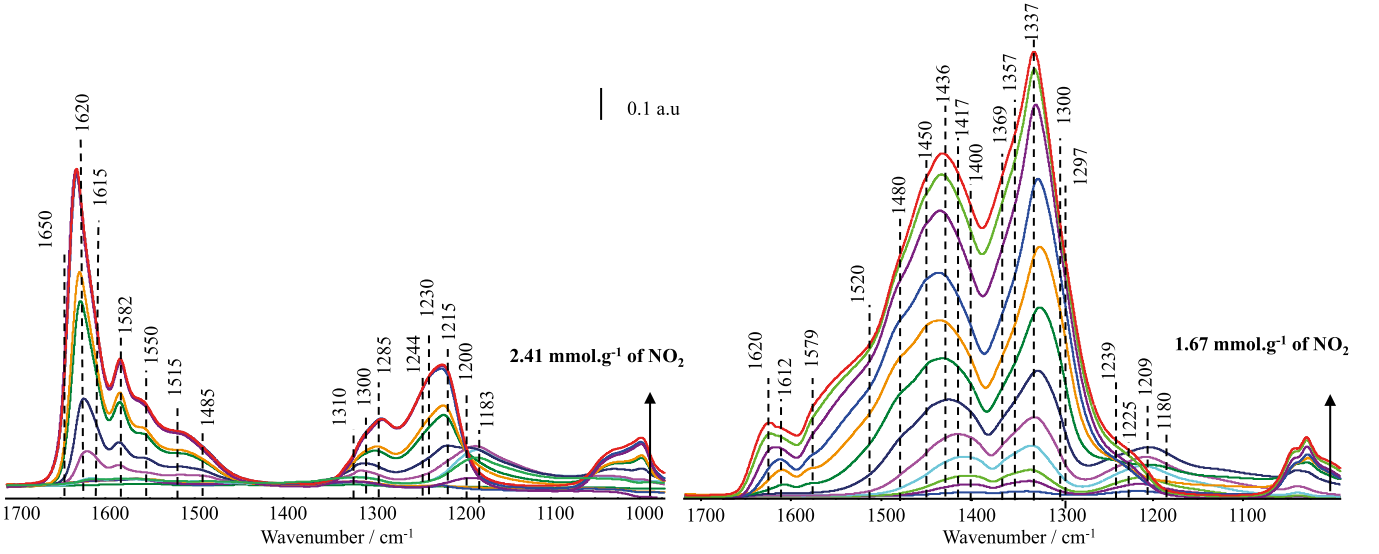

Fig. 4. Evolution of the spectra upon increasing NO_2 amount over ZrO_2-TiO_2 support (Left part) or Ba/ZrO_2-TiO_2 (Right part). Incremental doses of about 0.15 mmol g^{-1} were introduced till a value of about 1.7–2.4 mmol g^{-1} depending on the sample. (Note: NO_2 amounts indicated on the graph correspond to the value relative to the last spectrum shown, not to the saturation level of the catalysts).

further convert to NO_3^- while the band position allows its assignment to bridged NO_2^- over Zr or Ti sites. A pair of broad bands is also detected in the low coverage level range at about 1500–1305 cm^{-1} and a careful analysis of the spectra allows their decomposition into two distinct monodentate NO_3^- over Zr or Ti sites with degenerated ν_{as} modes at 1485–1310 and 1515–1300 cm^{-1} respectively. Another pair of bands at 1550–1285 cm^{-1} appears in the range of monodentate nitrates over Zr or Ti sites for intermediate NOx coverage level. For higher amounts of introduced NOx, several pairs of bands develop in parallel. Thus, the pair of peaks detected at 1582–1244 cm^{-1} and that at 1615–1230 cm^{-1} are both assigned to bidentate over Zr or Ti sites. Finally, in the bridged nitrates region, the TPD experiment (see spectra in Fig. SI3) evidenced that under evacuation between 373 and 473 K the peak at 1650 cm^{-1} increased at the expense of that at 1620 cm^{-1}. One thus proposes that bridged NO_3^- formed onto superficial Ti cations would migrate upon heating onto less accessible but more electropositive Zr sites. As a consequence, the pair of bands at 1650–1200 cm^{-1} is assigned to Zr bridged nitrates while that at 1620–1215 cm^{-1} would characterize bridged NO_3^- over Ti cations. Please refer to Table 1 for a summary of bands assignment.

As revealed on Fig. 4 right part, the nature of the NO_3^- species formed over pure ZT or over the Ba loaded catalyst is completely different and almost no trace of remaining ZT sites is detected once Ba is present. As the Ba nominal loading is similar for both oxide and taking into account that the specific area for ZT is half the one for Al_2O_3, it was indeed expected that the surface covering by Ba was higher for the ZT support.

The presence of Ba onto the ZT support leads to even more complex spectra than those observed for the Ba/Al_2O_3 formulation. However, it is again possible to evidence that the most striking feature for NO_2 adsorption over Ba/ZrO_2-TiO_2 consists in a pair of broad and intense bands at about 1440–1340 cm^{-1} that appear from the very first doses. The high wavenumber component of this split ν_{as} degenerated mode (about 1440 cm^{-1}) is completely absent for the bare ZrO_2-TiO_2 oxide and should thus characterize the barium phase. A careful analysis of the spectra even indicates that each broad component is indeed made of four peaks,

Table 2
Specific area (estimated from BET) and overall NOx adsorption capacity of various catalyst and oxide support estimated from the evolution of IR bands of NO_3^- and NO_2^- after NO_2 adsorption with or without heating at 653 K (spectra recorded at 293 K).

	Al_2O_3	Ba/Al_2O_3	ZrO_2-TiO_2	Ba/ZrO_2-TiO_2
Specific Area (BET)/$m^2\ g^{-1}$	200	200	100	100
NO_2 adsorbed	n/mmol g^{-1} (saturation)	n/mmol g^{-1} (saturation)	n/mmol g^{-1} (saturation)	n/mmol g^{-1} (saturation)
Non heated	/	1.48	/	1.41
Heated	1.35	1.07	1.81	1.68

so that finally four distinct species with the following IR signature 1480–1300, 1436–1369, 1417–1357 and 1400–1337 cm^{-1} are formed. The rather low extent of the ν_a split ($\Delta\nu_{as} < 180\ cm^{-1}$) suggests again that the corresponding species are either Ba monodentate nitrates or Ba polydentate nitrates while a more precise assignment was possible from the TPD data (see spectra in Fig. SI4). Indeed, the 1480–1300 cm^{-1} pair presents the lowest thermal stability as its intensity starts to decrease from 373 K. Then, the intensity of the 1400–1337 cm^{-1} pair also starts to decrease for evacuation temperatures above 473 K. The thermal stability range of the two last species is thus consistent with Ba monodentate NO_3^-. On the contrary, the species characterized by the 1436–1369 and 1417–1357 cm^{-1} pairs of bands resist to evacuation temperature as high as 673 K which is typical for bulk Ba polydentate (or ionic) nitrates.

In the same spectral range, a band was detected at 1450 cm^{-1} from the very first doses but its evolution could not be correlated with that of any other band. As a consequence, this lone peak was assigned to a Ba linear NO_2^-. Another type of nitrites, corresponding to a bridged species was detected at 1209 cm^{-1}. As the similar type of NO_2^- was observed at 1183 cm^{-1} for the Ba free ZT support, it suggests that the 1209 cm^{-1} is typical for a bridged species involving Ba site.

The remaining peaks are less easy to assign since their wavenumbers are close to those already observed for the Ba free ZrO_2-TiO_2. A similar methodology consisting in a heating at 653 K after each NO_2 dose was then undertaken in order to clarify which bands correspond to species involving the ZT support among the majority of peaks due to Ba species.

A clear heating effect was noticed in the high wavenumber range since the bands at 1620, 1612 and 1579 cm^{-1} almost vanished (spectra not shown). The expected redistribution of the Ba particles that renders the ZT support sites less and less exposed thus allows to conclude that bands at 1620, 1612 and 1579 cm^{-1} involve at least one ZT cation. A more precise study of the bands evolution upon Thermo Programmed Desorption experiments (see spectra in Fig. SI4) then provides the following assignments. The 1620–1225 and 1612–1180 cm^{-1} pairs of bands would characterize two distinct bridged NO_3^- involving either one Zr or Ti cation while the 1579–1297 cm^{-1} pair of band would be typical for a bidentate NO_3^- species on ZrO_2-TiO_2 perturbed by surrounding Ba.

On the contrary, the pair of band at 1520–1239 cm^{-1} almost kept an identical intensity with or without heating at 653 K and thus most probably characterizes a Ba NO_3^-. The intermediate extent of the ν_{as} split ($\Delta\nu_{as} = 280\ cm^{-1}$) suggests that the corresponding species are Ba bidentate nitrates. Please refer to Table 1 for a summary of the bands assignments relative to the whole species detected in the present work.

3.1.3. Quantitative comparison

As the detailed speciation of the various adsorbed NOx species would require the determination of the molar extinction coefficient for any individual species (out of the scope of this work), a global quantitative approach was adopted. As a consequence, the evolution of the integrated area of the whole bands within the [1700–1100 cm^{-1}] range as a function of the amount of introduced NO_2 in the cell was plotted. The intercept between the initial linear evolution and the plateau value (when the sample saturation was reached) allowed the estimation of the total amount of adsorbed NOx for various samples. It is worth noting that even if the ZT oxide support presents a smaller specific area when compared to the alumina support, the total amount of adsorbed NOx species after heating at 653 K is higher for the former (see Table 2). On the other hand, from the comparison of Figs. 2 and 4, the total area of IR bands appears to be larger for Al_2O_3 than for ZrO_2-TiO_2. It is thus obvious that direct relationship between the amount of adsorbed NOx and the total area of IR bands is not straightforward and complementary discussion regarding this point is provided in the SI file.

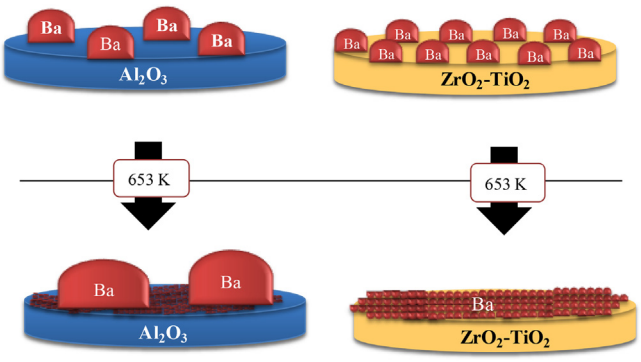

Scheme 1. A model for the evolution of the Ba support interaction upon heating under NO_2 atmosphere.

Table 3
Widely accepted range of values for Iso Electric Points of bare oxides from literature data.

Material	Formula	IEP
Alumina	Al_2O_3	8–9 [26,27]
Zirconium oxide	m-ZrO_2	5.5–6.5 [26]
Titanium oxide	TiO_2	4–6 [27]

Going with the comparison between the two supports, if one refers the amount of adsorption sites per area unit, one gets the following concentration for Al_2O_3: 6.75 10^{-6} mol m^{-2} and for ZrO_2-TiO_2: 1.81 10^{-5} mol m^{-2} thus making the ZT support the one with the highest sites density (about 3 times more).

It is thus suggested that the density of 'anchoring' sites for Ba upon barium loading is higher for the ZT oxide support: more finely dispersed Ba particles are thus expected for ZT when compared to Al_2O_3 (see Scheme 1). Considering the role of the acidity of the support on the Ba stabilization, it is indeed known that alumina is rather basic while both zirconia and titania are rather acidic (isoelectric point values reported in Table 3 below). From the point of view of the acid-base interaction strength, a higher stabilization of BaO over ZrO_2-TiO_2 is thus expected during the aqueous impregnation step. However, what is the most surprising here lies more in the much higher superficial density of anchoring sites on ZrO_2-TiO_2 than its stronger stabilization of the BaO phase."

Finally, considering the opposite evolution of the amount of adsorbed NO_2 after heating at 653 K for Ba/Al_2O_3 ($1.48 \rightarrow 1.07$ mmol g^{-1}) and for Ba/ZrO_2-TiO_2 ($1.41 \rightarrow 1.68$ mmol g^{-1}), one must conclude that the Ba particles 'evolution' proceeds in a very different way depending on the interaction with the oxide support.

The IR spectra indeed clearly indicate a change in the proportion of the adsorbed species upon heating (see Fig. 3 in the case of Ba/Al_2O_3), the amount of polydentate (or ionic) species becoming higher for both supports. Taking into account the stoichiometry for ionic $Ba(NO_3)_2$, it is obvious that moving from either monodentate, bidentate, or bridged to ionic nitrates should lead to an increase of the amount of adsorbed species. As a consequence, we propose that for alumina the Ba isolated 'medium size' clusters would mainly sinter into isolated big particles for which an important part of the bulk would remain unavailable (global amount of adsorption sites decreases upon heating) and part of Ba will move on the Al_2O_3 support while for the ZT oxide, the small isolated Ba particles would mainly spread over the whole support area to yield a fully covered surface onto which most of Ba adsorption sites are easily available (see Scheme 1). The thermal energy provided upon heating up to 653 K may however not be high enough to make the whole Ba sites available for NOx trapping even for the Ba/ZT formulation as indicated by its lower total adsorbed amount (1.68 mmol g^{-1}) compared to that for the bare support (1.81 mmol g^{-1}). An estimation of the Ba coverage level onto both supports and its evolution upon aging under NO_2 atmosphere was achieved from the integration of IR bands typical for interaction with the support only. The methodology is detailed in the Supplementary Information file and one obtains a 55% Ba coverage level over Al_2O_3 against 94% Ba coverage level over ZrO_2-TiO_2, values that are consistent with the model provided on Scheme 1.

Finally, it is worth noting that the Pt containing samples have also been *in situ* characterized through NO_2 adsorption and that the results are very similar both qualitatively and quantitatively. As a consequence, the nature of the formed species in presence of NO_2 under reaction conditions are expected to be similar, even if their relative proportion may change depending on the adsorption temperature.

3.2. *FTIR* operando *study of a long nitration period*

In most of the engine operating ranges, NO represents among NOx the most abundant species. That is the reason why, even if the presence of an upstream DOC catalyst generally converts part of NO into NO_2, most of the nitration studies deals with a lean flow made of NO and O_2. In the present study, aiming at clarifying the influence of the oxide support on the trapping efficiency of the Ba phase, it was however decided to test the nitration capacity of the catalysts using NO_2 in the lean flow. The reason is simple: if one wants to compare the nitration rate, it is of paramount importance to decorrelate the nitration step from the NO to NO_2 oxidation step that is often considered as the rate determining step, at least in the low temperature range [28–31]. Moreover, no traces of NO were detected during the first minute of *operando* reaction during which the whole amount of NO_2 was fully trapped. This indicates that in the present lean flow conditions, the presence of Pt does not lead to any dissociative adsorption of NO_2 that would lead to a mixture of NO and NO_2 in the gas phase and would thus prevent the qualitative comparison with the spectra obtained from the preliminary *in situ* study. Furthermore, in order to compare the catalysts at the limit of their working conditions, two extreme temperatures were tested, *i.e* either 473 K or 723 K.

The Fig. 5 represents the evolution of the cumulated amount of NOx trapped versus time on stream during a long nitration period (50 min) under NO_2, calculated from eq. 1 using the chemiluminescence data.

It is worth noting that for comparison purpose the experiments were performed using a similar amount of $Pt/Ba/Al_2O_3$ or $Pt/Ba/ZrO_2$-TiO_2 submitted to a similar flow (rate and composition). The left part of Fig. 5. represents the evolution of the trapped NOx in the full time on stream range. Focusing on one single catalyst, it is obvious that the shape of the curve depends on the adsorption temperature. For example, when the NO_2 adsorption was performed at 723 K (dotted line) over the $Pt/Ba/ZrO_2$-TiO_2 formulation, the total NOx trapped amount reaches quite fast a stabilized value (after about 600 s). On the contrary, when the adsorption was performed at much lower temperature (473 K, full line), the evolution presents a 'S' shaped curve presenting an inflexion point after about 1000 s. The analysis of the Al_2O_3 based formulation leads to the same qualitative conclusions when comparing the two extreme adsorption temperatures. For both samples, the 'S' shaped curves thus reveal distinct steps during the adsorption process associated with distinct 'global rates' as indicated by the different slopes before 500 s and after 1000 s. As widely reported in the literature, the NO_2 adsorption is known to go through nitrites formation that further convert into nitrates [8,31,32]. When the NO_2 adsorption is performed at low temperature, these two steps are kinetically decorrelated and NO_2^- first accumulate on the catalyst before starting to be converted to NO_3^-. In agreement with the IR spectra reported on Fig. 6, at 473 K, the first period of 'fast trapping' (before 500 s) would thus correspond to the storage of mostly superficial NO_2^- (bridged nitrite leads to the most intense IR peak for both samples). The almost flat transition period (between 500 s and 1000 s) would correspond to their oxidation into NO_3^- either form NO_2 (NO being detected in the exhaust gas during that period) or from O_2 (being present in large excess). The last period would finally correspond to the diffusion of superficial NO_3^- to the bulk of the trapping material (*i.e* Ba).

The NO_2^- formation from NO_2 adsorption can be considered as a non-activated step (low activation energy), as a consequence the kinetics for that step can be considered independent from the temperature. On the contrary, when the temperature increases till 723 K, the NO_2^- conversion into NO_3^- is highly kinetically favored and as a consequence the presence of NO_2^- is no more detected at the catalyst surface (see Fig. 6, higher part).

The goal of this paper is not to focus on the trapping mechanism and only a brief description is reported above in order to explain our data. However, there are proofs in the present manuscript that the NO_2 disproportionation leading to nitrate/nitrites does not proceed at first. For example, at 473 K during the very first minutes under stream (see Fig. 6) NO_2^- are the major species with only traces of NO_3^- are detected. If the NO_2 disproportionation reaction occurred, equal amounts of NO_2^- and NO_3^- should be detected according to the stoichiometry. As the consequence, our data are consistent with those obtained by Lietti et al. [33,34] who conclude that the most relevant route for NOx trapping is the nitrite one.

If the two catalysts are now compared at 723 K in the full time on stream range (Fig. 5 left part), it is obvious that the global curve shape is similar but that the time on stream required to reach a plateau is much higher for the Al_2O_3 based formulation when compared to the ZrO_2-TiO_2 one. The Fig. 5 also clearly indicates, whatever the adsorption temperature, that when submitted to a long period under NO_2, the two catalytic formulations do not differ significantly regarding their ability to store NOx (similar plateau values). Under flow conditions, the overall adsorption capacity for both formulations is thus similar (around 500 μmol g^{-1} at 473 K and around 250 μmol g^{-1} at 723 K) but the 'global' adsorption rate is much lower for the $Pt/Ba/Al_2O_3$ catalyst.

If the focus is now put on the comparison of the two catalysts in the low time on stream range (Fig. 5 right part), the

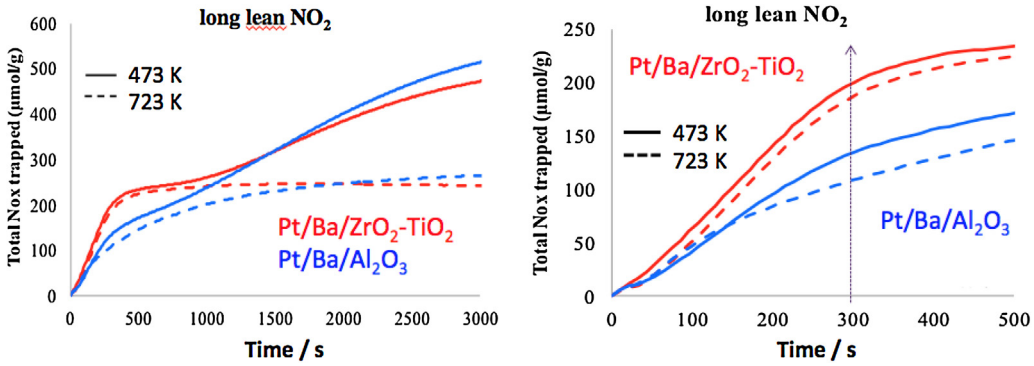

Fig. 5. Evolution of the cumulated adsorbed amount versus time on stream for both $Pt/Ba/Al_2O_3$ (blue curves) and $Pt/Ba/ZrO_2$-TiO_2 (red curves) submitted to a NO_2 flow at either 473 K (full lines) or 723 K (dotted lines). Left: full time on stream range (50 min). Right: enlargement during the first 500 s. (For interpretation of the references to colour in this figure legend, the reader is referred to the web version of this article.)

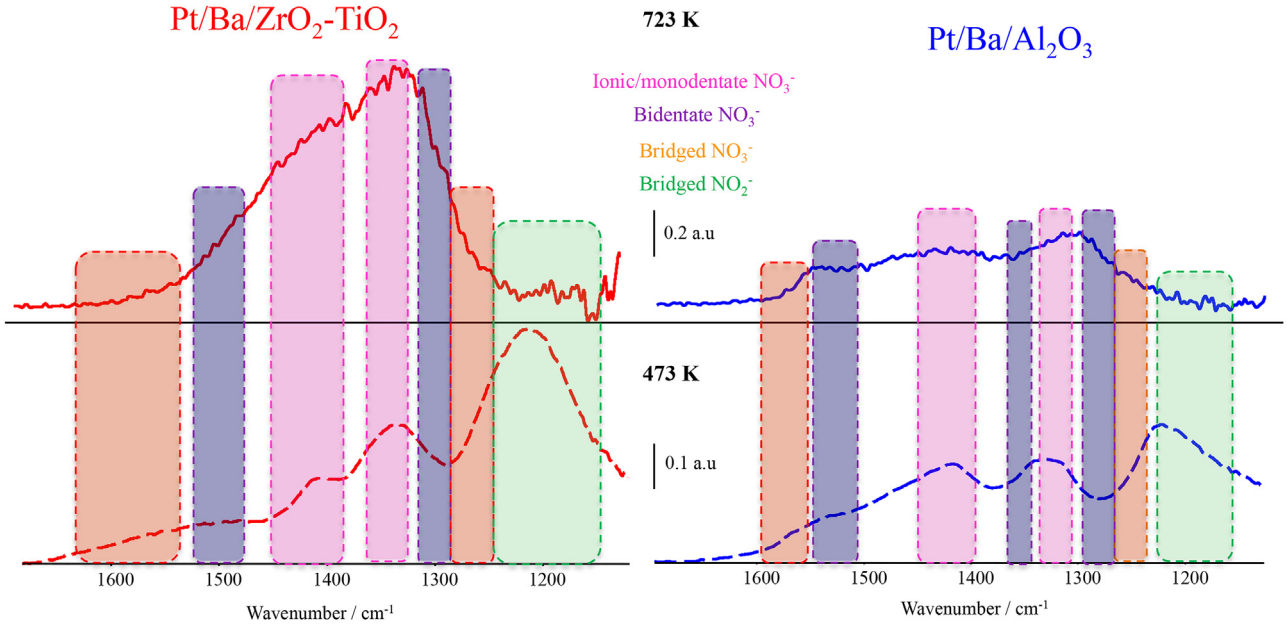

Fig. 6. IR spectra relative to $Pt/Ba/ZrO_2$-TiO_2 (left part) and $Pt/Ba/Al_2O_3$ (right part) after 300 s under lean flow at 473 K (lower part) or 723 K (upper part).

differences in the 'global' adsorption rate are even more obvious. Indeed, whatever the temperature, at a given time on stream below 500 s, the amount of trapped NOx is always much lower for the Al_2O_3 based formulation when compared to the ZrO_2-TiO_2 one. For example, after 300 s at 473 K, one gets amounts of adsorbed NOx of 130 $\mu mol\,g^{-1}$ for $Pt/Ba/Al_2O_3$ and 200 $\mu mol\,g^{-1}$ for $Pt/Ba/ZrO_2$-TiO_2 that lead to 'global' rates of about 0.43 $\mu mol\,g^{-1}\,s^{-1}$ and 0.67 $\mu mol\,g^{-1}\,s^{-1}$ respectively.

Regarding the nature of the adsorbed species, Fig. 6 showing the IR spectra obtained after 300 s under reaction flow indicates that at 473 K the peak relative to bridged NO_2^- species is the most intense one for both catalysts. The exact value of the molar extinction coefficient ε for the $\nu_a(NO_2^-)$ at about 1210–1220 cm^{-1} was not determined but taking into account that for $Pt/Ba/ZrO_2$-TiO_2 the total amounts of stored NOx after 300 s are similar at 473 K or 723 K (Fig. 5, bottom part), the comparison of the left part spectra of Fig. 6 allows here to conclude that $\varepsilon(NO_{2\_}) \approx \varepsilon(NO_{3\_})$ since the integrated area for both IR spectra are similar while only NO_3^- are present at 723 K. As a consequence, the most abundant adsorbed species at 473 K is confirmed to be NO_2^- for both catalytic formulations. A careful look at the ν_{as} (NO_2^-) peak position (about 1210–1220 cm^{-1}) furthermore reveals that Ba sites are involved for these nitrites formation (see Table 1). If one now compares the nitrite band intensity for both formulations at 473 K, it then appears that higher amount of Ba NO_2^- is formed over the ZrO_2-TiO_2 based catalyst than for the Al_2O_3 one. The lower values observed with $Pt/Ba/Al_2O_3$ for the total NOx trapped after 300 s thus arises form a lower availability of the Ba storing sites. Finally, even if majority, nitrites species are not the exclusive species formed at 473 K. Indeed, for both catalysts a pair of bands typical for monodentate and/or ionic NO_3^- is also detected. The preliminary *in situ* work revealed that such peaks were absent for the bare oxide support and thus they characterize nitrate over the barium phase. At 473 K, two shoulders are also detected for both catalysts above 1500 cm^{-1}. As concluded from the *in situ* part, they characterize traces of bidentate and bridged NO_3^- species formed over few remaining superficial sites from the oxide support.

After the same short duration (300 s) under NO_2, the nature of the adsorbed species at 723 K (Fig. 6 upper part) has changed. The thermal heat obviously provides the energy required for a fast and full conversion of the Ba nitrites into Ba nitrates. The intensity of the $\nu_{as}(NO_3^-)$ doublet for Ba NO_3^- is again much higher for Pt-Ba/ZrO_2-TiO_2 than for Pt-Ba/Al_2O_3 and even if the molar extinction coefficients are not directly comparable, it is obvious from the gas phase data (Fig. 5 right part) that the amount of trapped ionic Ba nitrates is much higher for the Pt-Ba/ZrO_2-TiO_2 catalyst. Finally,

and in agreement with the *in situ* results, the alumina support still does participate significantly to the storage as evidenced by the corresponding typical bidentate and bridged nitrates.

Aiming at summarizing the above data, it is worth noting that on the one hand, after a 300 s period under NO_2 at 723 K the amount of formed Ba bulk (or ionic) nitrates (monodentate species with similar IR feature being unstable at that temperature) is much higher over the Pt/Ba/ZrO_2-TiO_2 catalyst. On the other hand, the overall trapping capacity during a long lean period (about 50 min under NO_2) is similar for both formulations. These data provide evidences that Ba bulk (or ionic) nitrates form in a much faster way on the ZT based formulation. The presence of 'big' isolated Ba clusters on the Al_2O_3 based formulation would provoke a slow diffusion towards 'bulk' Ba adsorption sites while a rather thin layer of Ba covering 'entirely' the ZT area would enable a fast formation of Ba ionic nitrates (see scheme 1).

4. Conclusions

In the present work, the influence of the oxide support on the trapping efficiency of the Ba oxide storage phase was investigated. For the first time, two distinct catalytic formulations containing the same Pt and Ba nominal weight loading but using either an alumina or a mixed Zr-Ti oxide support were compared. The preliminary *in situ* IR characterization of the samples through NO_2 adsorption at 298 K and after heating at 653 K not only allowed to identify the nature of the various adsorbed species (nitrite and nitrate), their coordination mode (monodentate, bidentate, bridged or polydentate), their adsorption site (Ba phase or oxide support) but also that the ZT support presents a superficial sites density for NOx adsorption three time higher than the alumina one. As a consequence, it was suggested that the density of 'anchoring' sites for Ba upon barium loading is higher for the ZT oxide support: a higher amount of more finely dispersed Ba particles is thus expected for ZT when compared to Al_2O_3. In agreement with that hypothesis, the Ba loaded ZT formulation almost does not present remaining exposed superficial sites from the ZrO_2-TiO_2 support while on the contrary the Ba loaded alumina samples still leads to the significant formation of superficial aluminum nitrates.

The dynamic behavior of the samples was then tested upon nitration under flow using NO_2 at two extreme temperatures, *i.e* 473 K and 723 K. In agreement with our hypothesis of thinner Ba particles over the ZT support when compared with the alumina one, a short duration under NO_2 flow leads to a higher amount of Ba adsorbed NOx species (either NO_2^- at 473 K or NO_3^- at 723 K) over the Pt/Ba/ZrO_2-TiO_2 formulation. For long lean duration, the slow diffusion process inside the bigger Ba particles supported onto alumina may complete and finally the two samples reach similar level of total NOx trapped. The full storage capacity for both formulations is thus similar but under realistic NSR cyclic conditions for which the lean period typically remains below 300 s, the Pt/Ba/ZrO_2-TiO_2 will lead to a higher NOx adsorption efficiency related to a higher availability of the whole Ba sites.

Appendix A. Supplementary data

Supplementary data associated with this article can be found, in the online version, at http://dx.doi.org/10.1016/j.apcatb.2017.02.053.

References

[1] B. Pereda-ayo, J.R. González-velasco, in: S. Bari (Ed.), Diesel Engine Combust. Emiss. Cond. Monit., InTech, 2013, p. 266.
[2] N. Takahashi, H. Shinjoh, T. Iijima, T. Suzuki, K. Yamazaki, K. Yokota, H. Suzuki, N. Miyoshi, S. Matsumoto, T. Tanizawa, T. Tanaka, S. Tateishi, K. Kasahara, Catal. Today 27 (1996) 63–69.
[3] N. Miyoshi, S. Matsumoto, K. Katoh, T. Tanaka, Development of New Concept Three-Way Catalyst for Automotive Lean-Burn Engines, 1995.
[4] G. Liu, P.-X. Gao, Catal. Sci. Technol. 1 (2011) 552.
[5] A. William, S. Epling, L.E. Campbell, N.W. Currier, J.E. Parks, Catal. Rev. Sci. Eng. 46 (2004) 1–72.
[6] R.D. Clayton, M.P. Harold, V. Balakotaiah, AlChe J. 55 (2009) 687–700.
[7] F. Frola, F. Prinetto, G. Ghiotti, L. Castoldi, I. Nova, L. Lietti, P. Forzatti, Catal. Today 126 (2007) 81–89.
[8] B. Westerberg, E. Fridell, J. Mol. Catal. A Chem. 165 (2001) 249–263.
[9] A. Amberntsson, B. Westerberg, P. Engström, E. Fridell, M. Skoglundh, in: B.D. and G.F.F.B.T.-S. in S.S. and Catalysis (Ed.), Catal. Deactiv. 1999, Proc. 8th Int. Symp., Elsevier, 1999, pp. 317–324.
[10] S. Matsumoto, Y. Ikeda, H. Suzuki, M. Ogai, N. Miyoshi, Appl. Catal. B Environ. 25 (2000) 115–124.
[11] C. Sedlmair, K. Seshan, A. Jentys, J. Lercher, Catal. Today 75 (2002) 413–419.
[12] E. Fridell, H. Persson, L. Olsson, B. Westerberg, A. Amberntsson, Top. Catal. 16 (2001) 133–137.
[13] P. Engström, A. Amberntsson, M. Skoglundh, E. Fridell, G. Smedler, Appl. Catal. B Environ. 22 (1999) 241–248.
[14] N. Hachisuka, I. Yoshida, T. Ueno, H. Takahashi, SAE Tech. Pap. (2002).
[15] M. Piacentini, M. Maciejewski, A. Baiker, Appl. Catal. B Environ. 66 (2006) 126–136.
[16] M.Y. Smirnov, A.V. Kalinkin, D.A. Nazimov, A.V. Toktarev, V.I. Bukhtiyarov, Kinet. Catal. 56 (2015) 540–548.
[17] M. Corbetta, F. Manenti, C.G. Visconti, S. Pierucci, L. Lietti, AIDIC Conf. Ser. 11 (2013) 141–150.
[18] A. Carías-henriquez, S. Pietrzyk, C. Dujardin, Catal. Today 205 (2013) 134–140.
[19] N. Apostolescu, T. Schröder, S. Kureti, Appl. Catal. B Environ. 51 (2004) 43–50.
[20] J.H. Kwak, R.J. Chimentao, C.H.F. Peden, J. Phys. Chem. C 111 (2007) 2661–2669.
[21] L. Wu, S. Tong, M. Ge, J. Phys. Chem. A 117 (2013) 4937–4944.
[22] K. Hadjiivanov, Catal. Rev. Sci. Eng. 42 (2000) 71–144.
[23] T. Szailer, J.H. Kwak, D.H. Kim, J. Szanyi, C. Wang, C.H.F. Peden, Catal. Today 114 (2006) 86–93.
[24] J. Szanyi, J.H. Kwak, D.H. Kim, S.D. Burton, C.H.F. Peden, J. Phys. Chem. B 109 (2005) 27–29.
[25] J. Szanyi, J.H. Kwak, J. Hanson, C. Wang, T. Szailer, C.H.F. Peden, J. Phys. Chem. B 109 (2005) 7339–7344.
[26] H. Wakily, M. Mehrali, H.S.C. Metselaar, Eng. Technol. 47 (2010) 140.
[27] M.N. Rahaman, in: Marcel Dekker (Ed.), Ceramic Processing and Sintering, 2nd edition, CRC Press, New-York, 2003.
[28] S.S. Chaugule, A. Yezerets, N.W. Currier, F.H. Ribeiro, W.N. Delgass, Catal. Today 151 (2010) 291–303.
[29] M. AL-Harbi, W.S. Epling, Catal. Lett. 130 (2009) 121–129.
[30] I. Nova, L. Lietti, P. Forzatti, Catal. Today 136 (2008) 128–135.
[31] L. Castoldi, L. Righini, R. Matarrese, L. Lietti, P. Forzatti, J. Catal. 328 (2015) 270–279.
[32] P.J. Schmitz, R.J. Baird, J. Phys. Chem. B 106 (2002) 4172–4180.
[33] S. Morandi, F. Prinetto, G. Ghiotti, L. Castoldi, L. Lietti, P. Forzatti, M. Daturi, V. Blasin-aubé, Catal. Today 231 (2014) 116–124.
[34] L. Righini, L. Castoldi, L. Lietti, S. Sauce, P. Da Costa, P. Forzatti, Top. Catal. 56 (2013) 1906–1915.